INTERNATIONAL JOURNAL FOR NUMERICAL METHODS IN FLUIDS
Int. J. Numer. Meth. Fluids 2009; **61**:569–590
Published online 8 December 2008 in Wiley InterScience (www.interscience.wiley.com). DOI: 10.1002/fld.1969

Moving-boundary analysis of net vapor generation point in a steam generator

S. Paruya[1,*,†] and P. Bhattacharya[2]

[1]*Department of Chemical Engineering, National Institute of Technology, Durgapur 713 209, India*
[2]*Department of Chemical Engineering, Jadavpur University, Kolkata 700 032, India*

SUMMARY

This paper deals with the study of the dynamics of net vapor generation point in the boiling channel of the steam generator of Kaiga-1 nuclear power plant. The dynamics has been studied by perturbing liquid velocity at the inlet of boiling channel with a step function and heating rate with a ramp function. Both finite volume method (FVM) and finite difference method (FDM) have been applied to solve the model equations that have been developed to predict boiling boundary. The effect of thermal non-equilibrium conditions on subcooled boiling has been taken into consideration. A comparative study of the two methods has been carried out based on the analytical solution of the equations. The study shows that at higher system frequency, increasing number of computational grids increase the accuracy of numerical solutions using FVM while FDM fails to achieve the same. The superiority of FVM over FDM for the problem has also been confirmed by grid convergence analysis. An attempt has also been made to find the analytical solution of the effect of change of heat input on boiling boundary, which is an essential part of computations for the simulation of startup and shutdown of the steam generator. Copyright © 2008 John Wiley & Sons, Ltd.

Received 5 February 2008; Revised 14 October 2008; Accepted 15 October 2008

KEY WORDS: net vapor generation point; moving-boundary problem; boiling boundary; finite volume method; finite difference method; steam generator

1. INTRODUCTION

Movement of net vapor generation (NVG) point in the boiling channel of a steam–water natural circulation (SWNC) loop at various thermohydraulic conditions is an important moving-boundary phenomenon in which control volume in both two-phase steam–water region and single-phase water region changes with time in the event of dynamic changes of various operating conditions viz., heat flux, etc. This problem needs to be addressed for the plant transients such as startup and

*Correspondence to: S. Paruya, Department of Chemical Engineering, National Institute of Technology, Durgapur 713 209, India.
†E-mail: swapanparuya@rediffmail.com

shutdown of boilers. Thermohydraulic phenomena of SWNC loop in a steam generator system of nuclear power plants and thermal power plants is very complicated, particularly, during its startup and shutdown. This phenomena includes various unstable situations such as flow reversal, flow excursion, geysering effect and density-wave oscillation (Type-I and Type-II) [1, 2]. Several studies [3–8] show that an accurate model for boiling boundary needs to be incorporated in thermohydraulic models of SWNC loop for more realistic prediction of the phenomena.

Benedek and Drew [9] carried out frequency-domain analysis for the hydrodynamic effect on boiling boundary in a typical boiling channel using linear model with a major simplification that the phases remain at the state of thermal equilibrium at the boiling boundary. This assumption implying that the enthalpy of liquid reaches saturation value at the boundary may not be valid for real-time situations, particularly, during severe transients. Paruya *et al.* [3, 4] and Paruya and Bhattacharya [6] presented a simplified quasi-steady model for boiling boundary in natural circulation steam generator (NCSG) of an Indian nuclear reactor (Kaiga-1) to simulate reactor trip, feeder-pipe break and steam generator tube leakage. Frepoli *et al.* [10] achieved improved prediction of moving thermal quench back and forth in the core cooling during blowdown phase of large LOCAs by solving the model equations of the thermal-hydraulic code COBRA-TF/FHMG using finite volume method (FVM) with coarse meshing instead of finite difference method (FDM). van Bragt *et al.* [8] developed a linearized nodal time-domain boiling boundary model (second-order linear ODE) for predicting flashing-induced density instability of a two-phase natural circulation boiling water reactor at low pressures. Garea *et al.* [11] carried out theoretical investigation successfully using a moving-boundary nodal model to capture various instability phenomena in a boiling channel. Zhang and Zhang [12] studied the transient behavior of dry expansion evaporators in the vapor-compression refrigeration system developing a generalized moving-boundary model. The improved model successfully predicted void fractions and wall temperatures under unsteady conditions. Theoretical investigations [6, 7] of startup dynamics of SWNC loop suggest that the movement of NVG point strongly influences the dynamics of a SWNC loop during its startup. On the other hand, the prediction of dynamic instabilities such as geysering effect and density instabilities in the loop requires accurate tracking of NVG point. From these viewpoints, special attention is required for robust modeling approach for boiling boundary movement in the boiling channel of SWNC loop of NCSG at various conditions of flow.

Although a significant amount of work on moving boiling boundary problems have already been carried out, the literature survey [9, 13–15] shows that more realistic boundary conditions at NVG point (boiling boundary) are required for sharp tracking of the position of the interface between single-phase region and two-phase region. It is also needed to compare the performance of the numerical schemes to determine the suitability of the scheme to solve the present moving-boundary problem and other problems of similar nature. The boundary condition i.e. the liquid enthalpy at the boiling boundary has been improved instead of assuming the enthalpy at saturation. The boundary condition used in the present study accounts for the effect of thermal non-equilibrium at NVG point. The thermal non-equilibrium condition at the NVG point was experimentally confirmed by Saha and Zuber [16]. An extensive theoretical investigation on both hydrodynamic and thermal effect on the boiling height has also been presented in the paper to understand the complete dynamics of the boundary.

In view of the above, the moving-boundary problem of tracking NVG point has been studied by solving time-dependent PDEs with the help of FDM and FVM. The discretization of PDE using FVM and FDM has been done in such a way that it captures the motions of computational grids (called moving grids). Since FVM and FDM with very fine grids compete very closely in regard

DOI: 10.1002/fld

to the application to moving-boundary problems, as demonstrated in the paper, a comparison of the methods is essentially required to conclude about their performances. This has been made by carrying out an analysis of grid convergence with reference to the analytical solutions derived for the problem. While carrying out the comparison, due consideration was given to the fact that acceptable accuracy of the solutions has been achieved by FDM with finer meshing of channel geometry at the expense of greater computing time. On the other hand, FVM method is not only accurate in nature but also requires a less computing time because of the fact that the method is capable of handling coarse meshing of channel geometry.

During the discretization of the conservation equation using FVM, the differential equation is integrated over each of the control volumes in the computation domain, given a piecewise profile. In the present study, a piecewise linear profile has been assumed. Volume integrals of the advection term in PDE are converted to surface integrals using the divergence theorem. The numerical scheme of FVM essentially divides the domain into overlapping control volumes (grids), lending itself to direct physical interpretation [17–20]. As a result FVM becomes more conservative than FDM. The integration of the conservation equation during FVM-based discretization has been done using Leibnitz rule. The specific advantage of the rule in the moving-boundary problems is that it essentially accounts for the motion of control volume [21–24], which is particularly important in the present study. The rule is also capable of retaining the global conservation by satisfying the geometrical conservation law that states that the change in the domain volume in a time step must be equal to the volumetric changes along domain boundary. The method is computationally efficient because of maintaining an acceptable accuracy with coarse grids [8]. Another advantage of the FVM is that it can be easily formulated for unstructured meshes, leading to handle boundary conditions for unstructured shapes more accurately [25, 26]. These advantages of FVM have been exploited in many computational fluid dynamics packages.

FDM essentially approximates partial derivatives with the differences derived from the approximation of Taylor's series expansion based on discrete number of points in space. Although the numerical scheme of FDM can be utilized to cater to grid motions, it does not explicitly tell how the quantity varies between the grid points [20]. Thus, the implementation of FDM is relatively straightforward. When it is applied for structured rectilinear grids, the positions and connectivity of grid points need not be stored explicitly. This implicit connectivity and uniform grid-point spacing reduces memory use and simplifies computations. However, FDM suffers from several problems—(i) for uniform rectilinear grids, the fixed arrangement of grids in space requires high resolution in all locations to resolve high complexity in one location resulting in increased computation and memory, and (ii) FDM is also not so accurate and computationally efficient for the unstructured grids and for the situations in which one needs to handle the boundary conditions for irregular shapes. Automatic mesh refinement schemes do help in the situations at the cost of implementation complexity [27, 28].

2. FORMULATION FOR BOILING BOUNDARY COMPUTATION

Figure 1 presents a boiling channel in which a boiling boundary is shown at position $z=\lambda$. This position is assumed to be NVG point. NVG point is defined as a point along the axis of the boiling channel, at which a measurable amount of voids (steam bubbles) form under subcooled boiling conditions (Saha [29]). The region from $z=0$ to $z=\lambda$ has been assumed to be filled with water (by the definition of NVG point) and the region $z>\lambda$ with two-phase steam–water mixture. This

DOI: 10.1002/fld

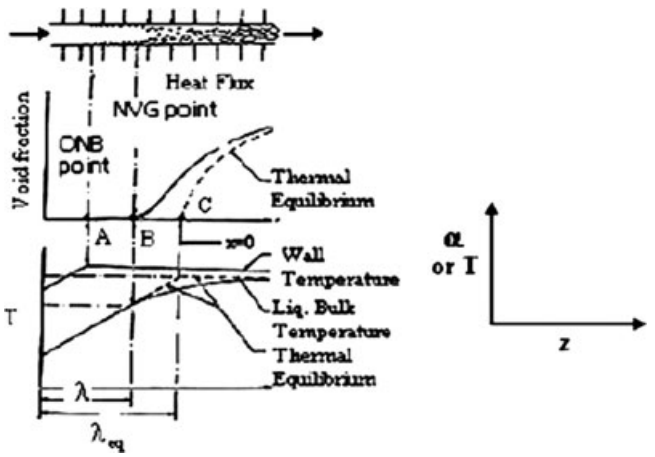

Figure 1. A typical boiling channel [29].

enables one to locate a sharp interface between the single-phase liquid and the mixture. Movement of this NVG point in the boiling channel depends on various thermal and hydraulic conditions of flow such as pressure, velocity, inlet enthalpy and heat input [7].

Modeling of boiling height (λ) requires to formulate mass balance equation (Equation (1)) and energy balance equation (Equation (2)) for single-phase liquid flow in the region from $z=0$ to $z=\lambda$. With the assumptions of insignificant viscous dissipation, negligible compressibility of liquid phase and constant pressure [13–15], the equations have been combined to set up the governing equation given by Equation (3).

Single-phase liquid mass balance:

$$\frac{\partial \rho_l}{\partial t}+\frac{\partial(\rho_l v_l)}{\partial z}=0 \tag{1}$$

Single-phase thermal energy balance:

$$\frac{\partial \rho_l h_l}{\partial t}+\frac{\partial(\rho_l h_l v_l)}{\partial z}=Q \tag{2}$$

Combining Equation (1)–(2), one gets

$$\frac{\partial h_l}{\partial t}+v_l\frac{\partial h_l}{\partial z}=q \quad \text{where } q=\frac{Q}{\rho_l} \tag{3}$$

It needs to be mentioned that as the compressibility of the liquid phase is negligible, the contribution of pressure change to the change of liquid enthalpy during startup and shutdown at low pressures is not significant. In order to reduce the complexity of the treatment, the effect of pressure change has not been brought in Equation (2). Consequently, pressure computation has been avoided in the present investigation. One may also note that as the startup and shutdown process progress through large velocity changes at a fast pace as a result of changing heating rate, molecular transport of momentum (which counts for viscous dissipation) is negligibly small compared with convective transport.

DOI: 10.1002/fld

3. ANALYSIS OF MOVING-BOUNDARY PROBLEM FOR HYDRODYNAMIC EFFECT ON BOILING BOUNDARY

As discussed in Section 1, the movement of NVG point is in the class of moving-boundary problems in which control volume changes with time, the treatment of the problem with FVM and FDM has been made in such a way that it essentially takes care of grid motions. The expressions of the grid motions have been explicitly derived. In order to study the hydrodynamic effect on the boiling boundary, v_l (liquid velocity at the inlet of the boiling channel) in Equation (3) has been varied with time following a step function while q, pressure p and inlet temperature T_i have been kept unchanged. The numerical schemes for solutions of Equation (3) along with the improved boundary conditions are discussed below.

3.1. FVM scheme

According to the FVM scheme [10], Equation (3) has been integrated over the entire single-phase liquid zone (from $z=0$ to $z=\lambda$ in Figure 2) by adding the integrals of N number of computation grids or nodes. For example, Equation (4) represents the integral for the second computation cell in Figure 2, in which z varies from $\lambda_1(t)$ to $\lambda_2(t)$

$$\int_{\lambda_1(t)}^{\lambda_2(t)} \frac{\partial h_l}{\partial t}\,\mathrm{d}z + \int_{\lambda_1(t)}^{\lambda_2(t)} v_l \frac{\partial h_l}{\partial z}\,\mathrm{d}z = \int_{\lambda_1(t)}^{\lambda_2(t)} q\,\mathrm{d}z \tag{4}$$

Using Leibnitz rule given by Equation (5), Equation (4) has been integrated based on the assumptions—(1) a quasi-steady state is assumed at the inlet boundary and outlet boundary of the single-phase zone, i.e. pressure and enthalpy at the inlet of heated channel and q are quasi-steady, (2) enthalpy change is piece-wise linear throughout the single-phase height (linear liquid temperature profile assumption of Levy [30]), i.e. enthalpy change is linear from inlet to NVG point indicating $h_{l\lambda}=h_i+N\Delta h$, and (3) every cell receives uniform and constant heat Q. This integration method has already been proved to be suitable for boiling system by several authors [3–5]. Leibnitz rule is expressed by

$$\frac{\mathrm{d}}{\mathrm{d}t}\int_{\lambda_1(t)}^{\lambda_2(t)} f(\lambda,t)\,\mathrm{d}z = f(\lambda_2,t)\frac{\mathrm{d}\lambda_2}{\mathrm{d}t} - f(\lambda_1,t)\frac{\mathrm{d}\lambda_1}{\mathrm{d}t} + \int_{\lambda_1(t)}^{\lambda_2(t)} \frac{\partial f(\lambda,t)}{\partial t}\,\mathrm{d}z \tag{5}$$

The term on the left-hand side of Equation (5) has been determined using mean-value theorem. Now, combining Equation (4) and (5), one obtains

$$\frac{\mathrm{d}\lambda_2}{\mathrm{d}t} = 2v_l - \frac{2q_(\lambda_2-\lambda_1)}{h_{l,2}-h_{l,1}} - \frac{\mathrm{d}\lambda_1}{\mathrm{d}t} \tag{6}$$

A general equation for nth computational node may be given by

$$\frac{\mathrm{d}\lambda_n}{\mathrm{d}t} = 2v_l - \frac{2q(\lambda_n-\lambda_{n-1})}{h_{l,n}-h_{l,n-1}} - \frac{\mathrm{d}\lambda_{n-1}}{\mathrm{d}t} \tag{7}$$

in which for computational node $n=N$, λ_N gives the estimate of boiling height. The detailed derivation of Equation (7) has been presented in the Appendix. The last term on the right hand of Equation (7) may be termed as velocity of the inlet boundary movement of nth node. The resulting set of N number of ODEs, as obtained from Equation (7) for N number of computation cells, has been solved simultaneously using implicit Euler method to find $\lambda_1, \lambda_2, \ldots, \lambda_N$.

DOI: 10.1002/fld

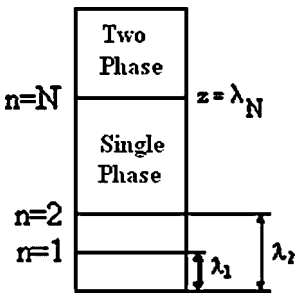

Figure 2. Computation cells in single-phase liquid zone (from inlet to NVG point).

3.2. FDM scheme

FDM scheme has been implemented based on the assumptions made in FVM scheme. The assumptions include—(1) quasi-steady state condition prevails at the inlet boundary and outlet boundary of the single-phase zone i.e. pressure and enthalpy at the inlet of heated channel and q are quasi-steady, (2) enthalpy change is piece-wise linear throughout the single-phase height [30] and (3) every cell receives uniform and constant heat Q.

In this scheme, Equation (3) has been discretized using FDM that assumes linear approximation of Taylor's series expansion of the enthalpy function $h_{ln}(\lambda_n, t)$ for nth node. The expansion is shown by Equation (8). The scheme was worked out by Benedek and Drew [9]

$$\frac{\partial h_{l,n}}{\partial t} + \frac{\partial h_{l,n}}{\partial \lambda_n}\frac{\mathrm{d}\lambda_n}{\mathrm{d}t} = \frac{\mathrm{d}h_{l,n}}{\mathrm{d}t} \tag{8}$$

Using the linear profile assumption of Levy [30] for liquid enthalpy, $\partial h_{l,n}/\partial \lambda_n$ is written as

$$\frac{\partial h_{l,n}}{\partial \lambda_n} = \frac{h_{l,n} - h_{l,n-1}}{\lambda_n - \lambda_{n-1}} \tag{9}$$

Now, from Equations (3), (8) and (9), one obtains

$$\frac{\mathrm{d}\lambda_n}{\mathrm{d}t} = v_l - \frac{q(\lambda_n - \lambda_{n-1})}{h_{l,n} - h_{l,n-1}} \tag{10}$$

A set of N number of ODEs, as obtained from Equation (10) for N number of computation nodes, has also been solved using implicit Euler method to find λ_N, which is the estimate of boiling height.

3.3. Boundary conditions

More realistic boundary conditions at the boiling boundary (NVG point) have been considered in the present investigation. Instead of assuming equilibrium boiling (saturated boiling) conditions at the boundary, as proposed by [9, 13–15], the correlations of Saha and Zuber [16], which cater to the effect of thermal non-equilibrium between phase and liquid phase, have been used to calculate more accurate liquid enthalpy at the boundary. Saha and Zuber experimentally verified the fact that subcooled boiling condition prevails at NVG point and proposed phenomenological correlations

DOI: 10.1002/fld

given by Equation (11) for a typical boiling channel. For both FVM and FDM, the enthalpy of liquid at NVG point $h_{l\lambda}$ has been calculated from the following equation:

$$h_{l\lambda} = h_{\text{sat}} - 0.0022 \frac{q''_w D_h c_{\text{pl}}}{k_l} \quad \text{if } Pe \leqslant 70\,000 \tag{11a}$$

$$h_{l\lambda} = h_{\text{sat}} - 154 \frac{q''_w}{\rho_l v_l} \quad \text{if } Pe > 70\,000 \tag{11b}$$

Peclet number Pe is defined by:

$$Pe = Re \cdot Pr = \frac{D_h v_l \rho_l c_{\text{pl}}}{k_l} \tag{11c}$$

3.4. Analytical solution for hydrodynamic effect on boiling boundary

The analytical solution of Equation (3) for λ_N has been worked out using the method of characteristics (MOC) [31]. The method is extensively used for the solution of the advection PDEs given by Equation (12). The term advection is defined as the transport of a scalar quantity in a vector field. For example, continuity equation for pipe flow is an advection PDEs

$$\frac{\partial \psi}{\partial t} + \nabla \cdot \psi v = 0 \tag{12}$$

The analytical solution of λ_N can be obtained by solving the following equation derived from Equation (3):

$$\frac{\mathrm{d}\lambda_N}{\mathrm{d}t} = v_l(t) - v_l(t-\tau) \tag{13}$$

The detailed derivation is presented in the Appendix. In Equation (13), τ is the transit time required by the liquid to travel from the inlet of boiling channel to the boiling boundary and it is calculated by dividing boiling height with the inlet velocity. One may deduce the transfer function $\lambda'_N(s)/v'_l(s)$ from Equation (13). The detailed mathematical manipulations are presented in the Appendix. The transfer function may be used to study the dynamics with various time-dependent velocity changes e.g. step changes.

4. ANALYSIS OF MOVING-BOUNDARY PROBLEM FOR THERMAL EFFECT ON BOILING BOUNDARY

It is extremely difficult to derive numerical solution of Equation (3) for boiling height, when the system under consideration is subjected to time-varying heating rate q at a constant v_l. For the case of time-varying q, nodal enthalpies vary with time. $\mathrm{d}h_2/\mathrm{d}t$ and $\mathrm{d}h_2/\mathrm{d}t$ cannot, therefore, be eliminated from Equation (A3) and need to be computed. But one may find difficulties to compute them from Equation (3) while computation of boiling boundary is the prime objective from the equation. In the present investigation, the thermal effect on the boiling boundary has been studied by ramping up q in Equation (3) keeping velocity unchanged. Substituting q in Equation (3) by

DOI: 10.1002/fld

$q(0)(1+\beta t)$, where β is slope of ramp input, and solving the resulting equation using MOC, one may obtain the final expression for boiling height, which is given by

$$\lambda(t) = v_l t + \frac{h_{l\lambda} - h_i - q(0)\left(t + \dfrac{\beta t^2}{2}\right)}{h_{l\lambda} - h_i}\lambda(0) \tag{14}$$

The analytical solution of this problem has been worked out in detail and it is presented in the Appendix. One may also note that the boiling height from Equation (14) has been determined with the boundary condition given by Equation (11).

5. RESULTS AND DISCUSSION

5.1. Description of nuclear steam generator loop

Kaiga-1 preheat steam generator (the schematic is presented in Figure 3) is a U-tube heat exchanger in which pressurized heavy water of primary heat transport unit flows through U-tubes and gives up heat to light water flowing in the shell side of the heat exchanger. The two legs of the U-tube bundle are known as hot leg and cold leg. At the hot leg heavy water is at relatively higher temperature than that at the cold leg. Demineralized feed water (approximately 90% of total feed water flow) is preheated in the heat exchanger called preheater located at the bottom of the cold leg. In the preheater section, the feed water flow is equally split into two parts. One half of the flow goes downward for mixing with the recirculating water from the down comer. The resulting mixture enters the lower riser (LRI) section (the main boiling section of the steam generator). The other half of the feed flow goes upward from the preheater and gets mixed with the steam–water mixture coming from the LRI of the steam generator and enters the upper riser (URI). Maximum heat transfer from the tube side to shell side takes place in this URI and a steam–water mixture with high void fraction exits from the top of the URI. The saturated water from steam drum is

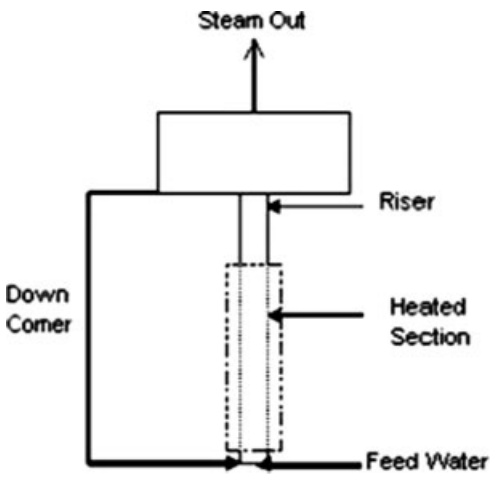

Figure 3. Steam–water flow circuit in NCSG of Kaiga-1 nuclear power plant.

DOI: 10.1002/fld

Table I. Geometrical configuration of loop.

Sl. no.	Item	Dimension
1	Steam drum length	4.585 m
2	Steam drum diameter	2.4 m
3	Length of upper riser section	10.07 m
4	Diameter of upper riser	1.343 m
5	Length of lower riser	2.04 m
6	Diameter of upper riser	1.343 m
5	Down comer length	12.11 m
6	Down comer diameter	0.8320 m

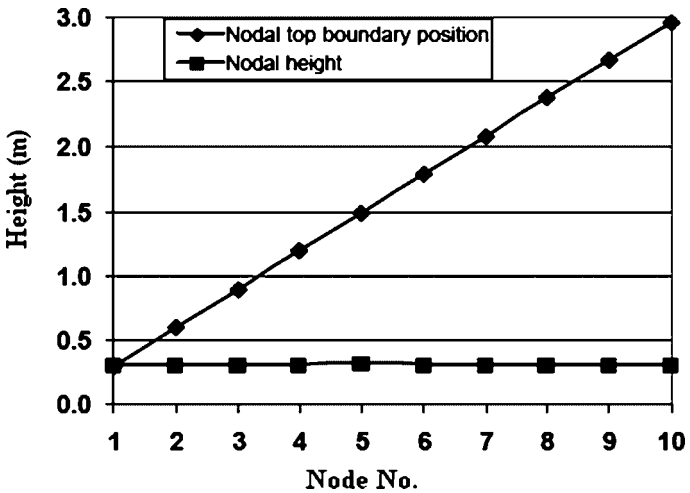

Figure 4. Initial nodal heights and nodal top boundary positions.

recirculated through the down comer after mixing with about 10% feed water (auxiliary feed) and reheated drain flow in the upper section of the down comer.

5.2. Dynamics of boiling boundary

5.2.1. Hydrodynamic effect on boiling boundary. With the configuration of natural circulation steam generator (NCSG), which is presented in Figure 3 and Table I, the results of the hydrodynamic effect on the boiling boundary are presented here based on FVM, FDM and exact solution. Initial values of nodal heights were shown in Figure 4, which were calculated from either Equation (7) or Equation (10) under steady-state conditions of pressure of 6.0 bar and inlet temperature of 25°C. Initial value of v_l was 6.16×10^{-3} m/s. The steady-state value of q was calculated to be 142.9 W/kg. The velocity calculated from first principle [7] is very low at the initial phase of NCSG startup due to the fact that the buoyancy force in the SWNC loop is not so significant because of low heating rate. It may be noted that the thermo-physical properties of light water were used in the present investigation. To study the hydrodynamic effect, a positive step change (30%) of circulation velocity at the inlet of boiling channel was impressed under constant heat

DOI: 10.1002/fld

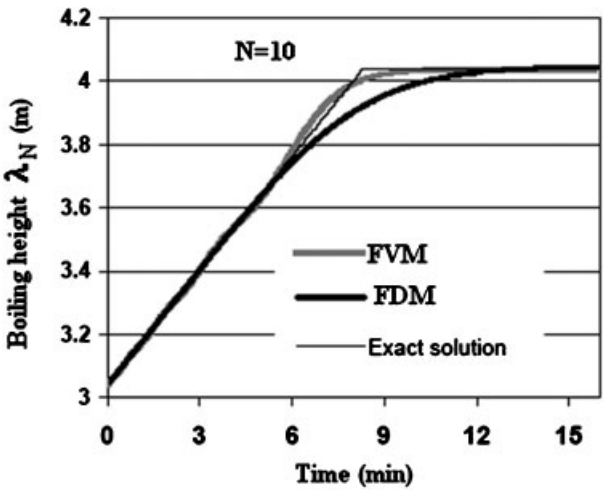

Figure 5. Response of boiling height using FVM, FDM and exact solution for 30% step change of inlet velocity for $N = 10$.

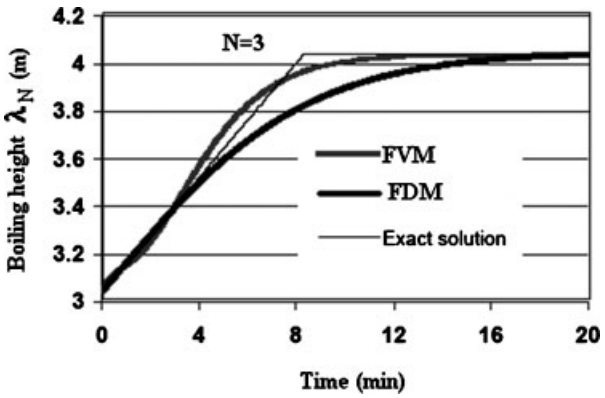

Figure 6. Response of boiling height using FVM, FDM and exact solution for 30% step change of inlet velocity for $N = 3$.

input of 142.9 W/kg, constant inlet temperature of 25°C and constant system pressure of 6.0 bar. This step change was effected by decreasing flow resistance.

Figure 5 presents the time-dependent variations of boiling height computed with FVM, FDM and exact solution for $N = 10$. Numerical results indicate that maximum deviations from exact solutions for FVM and FDM have been found to be 0.62 and 2.88%, respectively. Figure 6 shows the variation of boiling height with time for $N = 3$ and the corresponding deviations are 2.11 and 5.34%. Figures 5 and 6 also show that the numerical solutions are very close to exact solutions at lower frequencies (when the circulation velocity is low) and the solutions differ appreciably at higher frequencies. It is interesting to note that the solutions obtained by FVM are reasonably closer to the exact solution, compared with the solutions obtained by FDM. Therefore, one can

DOI: 10.1002/fld

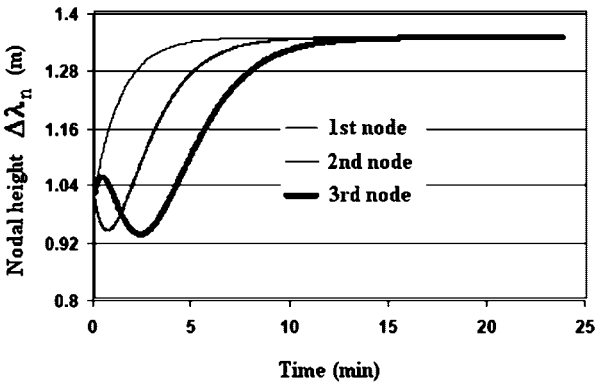

Figure 7. Response of nodal height using FVM for 30% step change of inlet velocity for $N=10$.

conclude that exact solutions at higher system frequencies can be satisfactorily approximated by FVM with increased value of N of 10 while FDM fails to yield reasonably accurate results. It is also important to mention that the system experiences higher frequencies when the effect of the step change in velocity has reached to the boiling boundary. Therefore, the analysis establishes the fact that it is required to compare the solutions for the transient responses of a system for choosing a suitable numerical method. While comparing the steady-state results, uncertainties of the numerical methods may sometimes be very less and may be, therefore, sometimes misleading to adopt a suitable numerical method for a system.

Figure 6 describes the response of nodal height adaptations ($\Delta\lambda_n=\lambda_n-\lambda_{n-1}$) using FVM for $N=3$. No oscillation is found in the first node and the effect of velocity change is experienced immediately in the node. In the nodes ($n>1$), the out-of-phase oscillations of nodal adaptations are seen. These out-of-phase oscillations are due to the transportation delay for individual node. The delay is the transit time required by the liquid to travel from the inlet of boiling channel to the nodal upper boundary and it can be calculated by

$$\tau_n=\frac{\lambda_n}{v} \tag{15}$$

The oscillations appearing for the higher-order ODEs for higher nodes are due to the fact that nodal computations in FVM are strongly dependent on the relative velocity between the velocity of inlet boundary movement ($\mathrm{d}\lambda_{n-1}/\mathrm{d}t$) and the fluid velocity at inlet boundary (v_l) as is evident from Equation (7). For the first node, $\mathrm{d}\lambda_{n-1}/\mathrm{d}t$ is zero because of the fixed inlet boundary, whereas nonlinear changes of $\mathrm{d}\lambda_{n-1}/\mathrm{d}t$ with time are observed for higher nodes. It is important to note that in Figure 7 the oscillations of nodal adaptations continue for the time equal to the transit time of fluid for the individual node. After the transit time τ_{n-1} of previous node $(n-1)$ elapses, the oscillation disappears for each node (n). This is because of the fact that the velocity of inlet boundary movement becomes zero ($\mathrm{d}\lambda_{n-1}/\mathrm{d}t=0$) after the corresponding transit time for $n-1$ node. One may also note that in Figure 7 when the τ_{n-1} is over, the nodal height of nth node starts to increase monotonically to a steady-state value following the dynamics of a first-order system subjected to a step change in input. Therefore, it is evident that in a moving-boundary problem analyzed with the help of FVM, the nodes ($n>1$) experience the effect of velocity of inlet boundary prior to the direct effect of step change in fluid velocity. Figures 8–12 present the response of nodal

DOI: 10.1002/fld

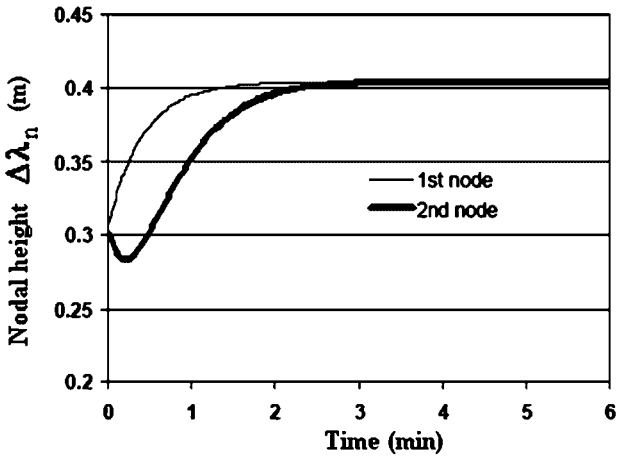

Figure 8. Response of nodal height using FVM for 30% step change of inlet velocity for $N = 10$.

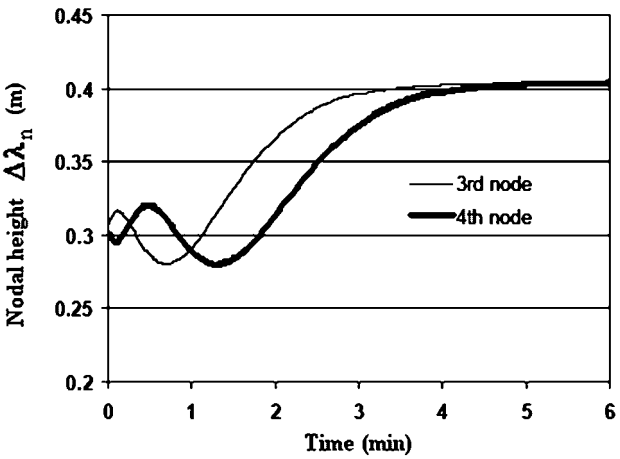

Figure 9. Response of nodal height using FVM for 30% step change of inlet velocity for $N = 10$.

height adaptations using FVM for $N = 10$. Similar nature of oscillations as discussed is found for this case. Figure 13 presents the response of the nodal top-boundary position of each node for $N = 10$. The time corresponding to the peak value (may be called as peak time) increases from lower nodes to higher nodes.

Contrary to FVM, FDM scheme does not account for the effect of velocity of inlet boundary in the nodal computations. The solutions for nodal heights using FDM scheme shown in Figure 14 are not oscillatory in nature. All the nodal height responses follow the first-order dynamics with time delay except for the first node that experiences the effect of velocity change without time delay.

DOI: 10.1002/fld

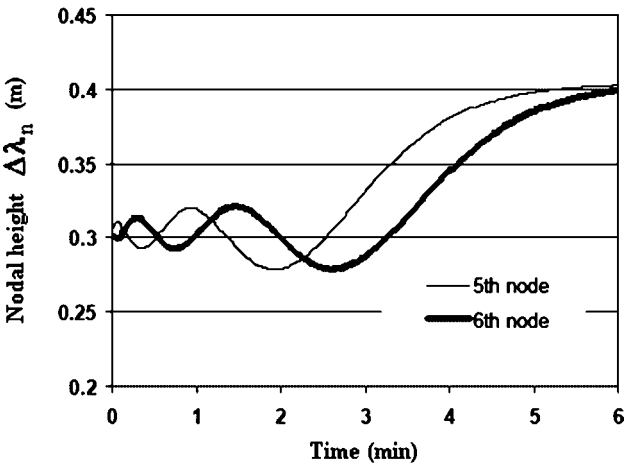

Figure 10. Response of nodal height using FVM for 30% step change of inlet velocity for $N = 10$.

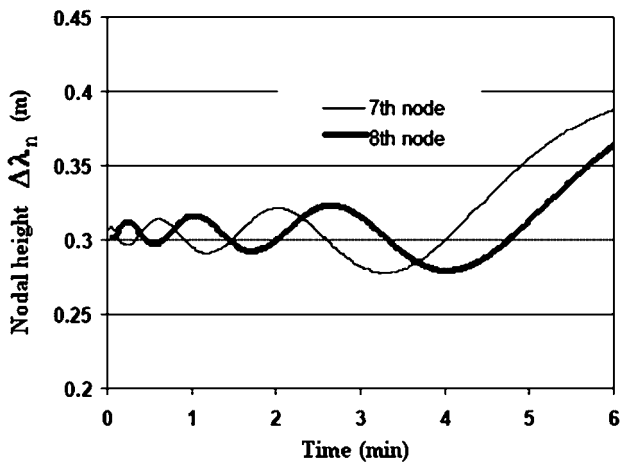

Figure 11. Response of nodal height using FVM for 30% step change of inlet velocity for $N = 10$.

5.2.2. Analysis of grid convergence. The order of grid convergence is defined as the difference between the numerical solution and the exact solution,

$$E = f(\Delta z) - f_{\text{exact}} = C(\Delta z)^{\eta} + \text{HOTs} \tag{16}$$

where C is a constant, Δz is the measure of grid spacing and η is the order of convergence. HOTs are the higher-order terms. A second-order convergence has η equal to two. The order of grid convergence determines the behavior of the solution error. Although a CFD code uses a numerical algorithm to provide a theoretical order of convergence, the effect of the boundary conditions, numerical models and grid reduce this order and the observed order of convergence will likely

DOI: 10.1002/fld

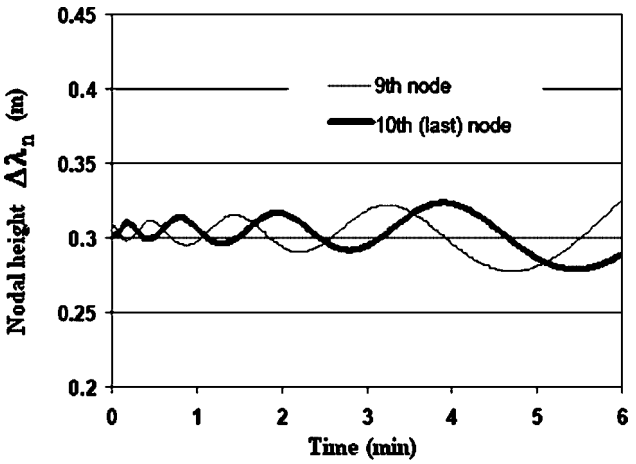

Figure 12. Response of nodal height using FVM for 30% step change of inlet velocity for $N = 10$.

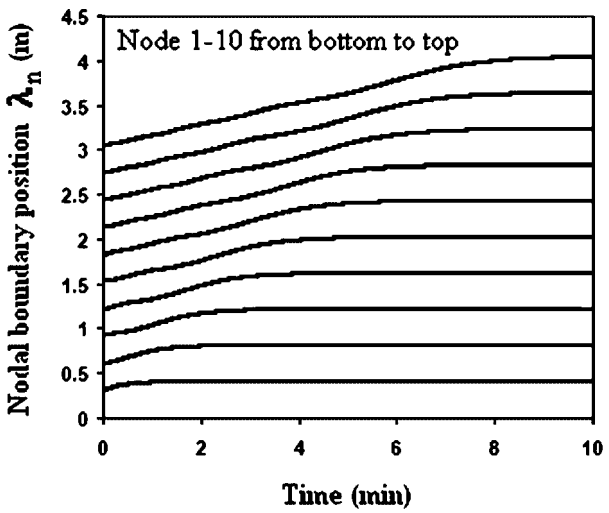

Figure 13. Response of nodal boundary using FVM for 30% step change of inlet velocity for $N = 10$.

be lower than the theoretical order. Methods for examining the grid and temporal convergence of CFD simulations are discussed by Roache [32].

Neglecting HOTs in Equation (16) and taking the logarithm on both sides of the equation, one may obtain the following equation:

$$\log(E) = \log(C) + \eta \log(\Delta z) \tag{17}$$

The order of convergence η can be obtained from the slope of the curve of $\log(E)$ versus $\log(\Delta z)$. If such data points are available, the slope (η) can be computed from a least-square fit of the data.

DOI: 10.1002/fld

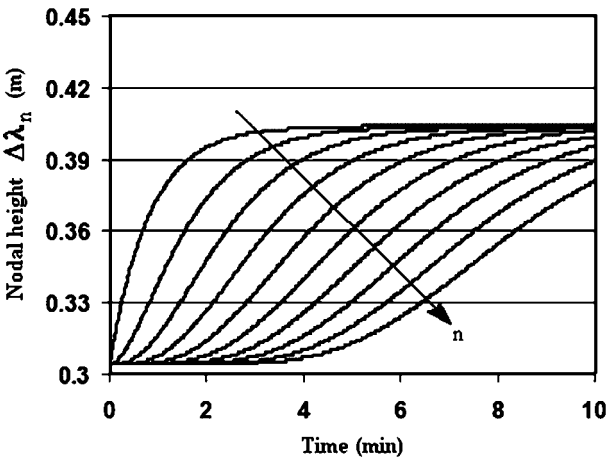

Figure 14. Nodal height variation with time using FDM for 30% step change of inlet velocity for $N=10$.

However, the algorithm is not as efficient as expected because of the fact that both the simplification by neglecting HOTs and the least-square fit introduce some uncertainties in determining the order.

A more direct evaluation of η, as discussed by Roache [32], can be obtained from three solutions using a constant grid refinement ratio r. The expression for η is given by

$$\eta = \frac{\log\left(\dfrac{f_4 - f_2}{f_2 - f_1}\right)}{\log(r)} \tag{18}$$

where, f_1, f_2 and f_4 are the degrees of closeness of numerical solutions to the exact solution $(1-E_N)$ corresponding to the normalized grid spacing 1, 2 and 4. E_N is the error of numerical solution obtained from Equation (19). Table II presents values of E_N at various normalized grid spacing for a run of 500 s

$$E_N = \left| \frac{\lambda_{N,\text{exact}} - \lambda_N}{\lambda_{N,\text{exact}}} \right| \tag{19}$$

Using Equation (18) and grid refinement ratio (r) of 2 obtained from normalized grid spacing Table II, the observed η has been calculated to be 1.379 and 0.943 for FVM and FDM, respectively The observed order of grid convergence indicates that FVM is superior to FDM in regard to grid convergence and accuracy. FDM shows first-order convergence. This can also be confirmed by the non-oscillating variation of error with time for FDM and the oscillating variation of error with time for FVM. The variations are presented in Figure 15. The errors of FVM (Table II) indicate that for coarse grids, FVM shows higher-order accuracy, establishing the facts that the method is more conservative than FDM and more computationally efficient. It is also important to note that with fine grids ($N=40$), both the methods yield the same order of accuracy.

5.2.3. Thermal effect on boiling boundary. As mentioned earlier, the thermal effect on the boiling boundary was studied by ramping up the heating rate (W/kg). The analytical solutions given by Equation (14) are presented in Figure 15 for $\beta=0.001, 0.01$ and 0.1. It is reflected from Figure 16

DOI: 10.1002/fld

Table II. Grid convergence analysis for a run of 500 s.

No. of grid (N)	Normalized grid spacing ($=N_{\max}/N$)	FVM error, E_N	FDM error, E_N	FVM solution, λ_N	FDM solution, λ_N	Exact solution, $\lambda_{N,\text{exact}}$
10	4	0.009635	0.010156	3.877	3.801	3.84
20	2	0.002865	0.003646	3.851	3.826	3.84
40	1	0.00026	0.00026	3.841	3.839	3.84

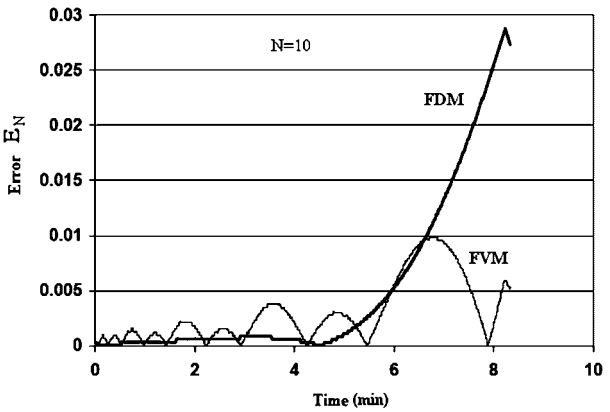

Figure 15. Temporal variation of error for FVM and FDM.

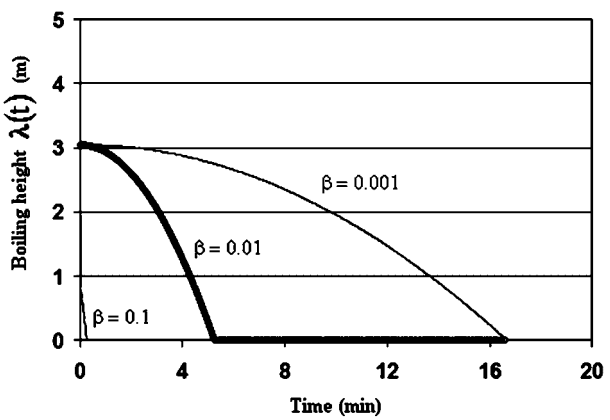

Figure 16. Thermal effect on the boiling height at constant inlet velocity.

that the boiling channel experiences the effect of the change in heating rate without any time delay. The boiling height decreases fast with the increase in heating rate. One may anticipate that the slope β has a critical value above which the solution will be unstable. It is important that care must be taken while carrying out the startup operation of a steam generation unit by ramping up heating rate.

DOI: 10.1002/fld

6. CONCLUSIONS

The above theoretical investigation of the moving-boundary problem is very much relevant to the startup phase of NCSG and FVM has been proved to be a sound scheme to solve the problem. This FVM can be preferentially used in the complicated situations where the exact solutions are difficult to obtain. During severe transients such as startup or shutdown, FDM with $N=10$ fails to secure reasonably accurate solution that is obtained by FVM (Figure 4) because of more conservative formulation with FVM which essentially considers grid volume rather than grid point. With even finer grids, $N=40$, as is evident from Table II, the two methods closely compete. Grid convergence analysis and Table II establish the facts that FVM has higher order of grid convergence and is more computationally efficient than FDM. Temporal variation of error (E_N) and nodal height ($\Delta\lambda_n$) in FVM follows second-order dynamics while the same in FDM follows a first-order dynamics. The optimization for compromising among solution accuracy, solution stability and computational load (CPU time) may be made for the better performance of FVM, although the same is true for any numerical simulation to be more efficient. This is much important for real-time simulation. It has been observed by numerical experiment that the optimum number of computational nodes strongly depends on the critical frequency defined as the ratio of inlet velocity to initial boiling height. Study on the thermal effect on the boiling boundary indicates that unlike the hydrodynamic effect, the effect of change in heating rate on the boiling height is instant, i.e. boiling height changes without any time delay. Since at the critical heating rate corresponding to the critical value of β the solution becomes unstable, it can be recommended that heating rate should be adjusted so as to remain below this critical value. It is also required to compare the computation results with experimental data or the data using sophisticated CFD packages.

APPENDIX A: CALCULATION OF BOILING BOUNDARY USING FVM

Equation (3) is integrated applying Leibnitz integral rule for $i=1$ to 2

$$\int_{\lambda_1(t)}^{\lambda_2(t)} \frac{\partial h_1}{\partial t}\,\mathrm{d}z + \int_{\lambda_1(t)}^{\lambda_2(t)} v_1 \frac{\partial h_1}{\partial z}\,\mathrm{d}z = \int_{\lambda_1(t)}^{\lambda_2(t)} q\,\mathrm{d}z \tag{A1}$$

Leibnitz integral rule is

$$\frac{\mathrm{d}}{\mathrm{d}t}\int_{\lambda_1(t)}^{\lambda_2(t)} f(\lambda,t)\,\mathrm{d}z = f(\lambda_2,t)\frac{\mathrm{d}\lambda_2}{\mathrm{d}t} - f(\lambda_1,t)\frac{\mathrm{d}\lambda_1}{\mathrm{d}t} + \int_{\lambda 1(t)}^{\lambda 2(t)} \frac{\partial f(\lambda,t)}{\partial t}\,\mathrm{d}z \tag{A1a}$$

Defining $h_1=h_1(\lambda_1)$ and $h_2=h_1(\lambda_2)$ and substituting h_1 and h_2 in the result of integration, one gets

$$\frac{\mathrm{d}}{\mathrm{d}t}\int_{\lambda_1}^{\lambda_2} h\,\mathrm{d}z - h_2\frac{\mathrm{d}\lambda_2}{\mathrm{d}t} + h_1\frac{\mathrm{d}\lambda_1}{\mathrm{d}t} + v_1h_2 - v_1h_1 = q(\lambda_2-\lambda_1) \tag{A2}$$

Substituting the linear-average value of $h(h=(h_l+h_2)/2)$, one obtains

$$h\left(\frac{\mathrm{d}\lambda_2}{\mathrm{d}t} - \frac{\mathrm{d}\lambda_1}{\mathrm{d}t}\right) + \frac{\lambda_2-\lambda_1}{2}\left(\frac{\mathrm{d}h_2}{\mathrm{d}t} + \frac{\mathrm{d}h_1}{\mathrm{d}t}\right) - h_2\frac{\mathrm{d}\lambda_2}{\mathrm{d}t} + h_1\frac{\mathrm{d}\lambda_1}{\mathrm{d}t} + v_lh_2 - v_1h_l = q(\lambda_2-\lambda_1) \tag{A3}$$

DOI: 10.1002/fld

For a constant q as assumed,

$$\frac{\mathrm{d}h_2}{\mathrm{d}t}=\frac{\mathrm{d}h_1}{\mathrm{d}t}=0 \tag{A4}$$

From Equations (A3) and (A4), one gets

$$\frac{h_1+h_2}{2}\left(\frac{\mathrm{d}\lambda_2}{\mathrm{d}t}-\frac{\mathrm{d}\lambda_1}{\mathrm{d}t}\right)-h_2\frac{\mathrm{d}\lambda_2}{\mathrm{d}t}+h_1\frac{\mathrm{d}\lambda_1}{\mathrm{d}t}=v_1(h_1-h_2)+q(\lambda_2-\lambda_1) \tag{A5}$$

or

$$(h_2-h_1)\frac{\mathrm{d}\lambda_2}{\mathrm{d}t}-(h_2-h_1)\frac{\mathrm{d}\lambda_1}{\mathrm{d}t}=-2v_1(h_1-h_2)-2q(\lambda_2-\lambda_1) \tag{A6}$$

Finally,

$$\frac{\mathrm{d}\lambda_2}{\mathrm{d}t}+\frac{\mathrm{d}\lambda_1}{\mathrm{d}t}=2v_1-\frac{2q(\lambda_2-\lambda_1)}{h_2-h_1} \tag{A7}$$

Integration from node n to node $n+1$ results in

$$\frac{\mathrm{d}\lambda_{n+1}}{\mathrm{d}t}=2v_1-\frac{2q_w(\lambda_{n+1}-\lambda_n)}{h_{n+1}-h_n}-\frac{\mathrm{d}\lambda_n}{\mathrm{d}t} \tag{A8}$$

APPENDIX B: ANALYTICAL SOLUTION OF BOILING BOUNDARY FOR TIME-DEPENDENT VELOCITY (METHOD OF CHARACTERISTICS)

$$\frac{\partial h}{\partial t}+v(t)\frac{\partial h}{\partial z}=q,\quad 0\leqslant z\leqslant\lambda(t) \tag{B1}$$

For moving boiling boundary, $z(0)=\lambda(0)$.

BC: $h(0,t)=h_i$

IC: $h(z,0)=h_i+az$

Linear profile of enthalpy has been assumed as mentioned earlier. h_i is enthalpy at channel inlet.

According to the definition of $h=h(z,t)$, one can write

$$\frac{\mathrm{d}h}{\mathrm{d}t}=\frac{\partial h}{\partial t}+\frac{\partial h}{\partial z}\left(\frac{\mathrm{d}z}{\mathrm{d}t}\right) \tag{B2}$$

Comparing Equation (B1) and Equation (B2)

$$\frac{\mathrm{d}h}{\mathrm{d}t}=q \tag{B3}$$

$$\frac{\mathrm{d}z}{\mathrm{d}t}=v(t) \tag{B4}$$

Integrating Equation (B4), one gets

$$z(t)=\int v(t)\,\mathrm{d}t+c_2 \tag{B5}$$

c_2 is integration constant.

DOI: 10.1002/fld

Now the time-dependent change of boiling boundary is given by

$$\frac{\mathrm{d}\lambda}{\mathrm{d}t}=\left.\frac{\mathrm{d}z}{\mathrm{d}t}\right|_{t}-\left.\frac{\mathrm{d}z}{\mathrm{d}t}\right|_{t-\tau}=v(t)-v(t-\tau) \tag{B6}$$

τ accounts for transportation delay and is defined by $\lambda(0)/v(0)$. Taking Laplace transform of Equation (B6), one obtains

$$\frac{\lambda'(s)}{v'(s)}=\frac{1-\mathrm{e}^{\tau s}}{s} \tag{B7}$$

APPENDIX C: EXACT SOLUTION OF BOILING BOUNDARY FOR TIME-DEPENDENT HEAT INPUT (METHOD OF CHARACTERISTICS)

q is ramped up according to $q(0)(1+t)$.

Replacing q by $q(0)(1+t)$ and h_1 by h in Equation (3), one obtains

$$\frac{\partial h}{\partial t}+v\frac{\partial h}{\partial z}=q(0)(1+t),\quad 0\leqslant z\leqslant\lambda(t) \tag{C1}$$

IC: $h(z,0)=h_i+az$

BC: $h(0,t)=h_i$

According to the definition of $h=h(z,t)$, one can write

$$\frac{\mathrm{d}h}{\mathrm{d}t}=\frac{\partial h}{\partial t}+\frac{\partial h}{\partial z}\left(\frac{\mathrm{d}z}{\mathrm{d}t}\right) \tag{C2}$$

Comparing Equation (C1) and Equation (C2)

$$\frac{\mathrm{d}h}{\mathrm{d}t}=q(0)(1+t) \tag{C3}$$

$$\frac{\mathrm{d}z}{\mathrm{d}t}=v \tag{C4}$$

Integrating Equation (C3)

$$h(z,t)=q(0)\left(t+\frac{t^2}{2}\right)+c_1 \tag{C5}$$

c_1 is integration constant. Using $h(z(0),0)$, c_1 is given by

$$c_1=h(z(0),0)=h(\lambda(0),0) \tag{C6}$$

Integrating Equation (C4), one gets

$$z(t)=vt+c_2 \tag{C7}$$

Putting $z(0)=\lambda(0)$ (say) in Equation (C7)

$$c_2=\lambda(0) \tag{C8}$$

DOI: 10.1002/fld

From Equations (C7) and (C8), one may obtain

$$z(t)-vt=\lambda(0) \tag{C9}$$

From Equations (C6) and (C9), one may also obtain

$$c_1=h(z(t)-vt,0) \tag{C10}$$

From Equations (C5), (C9) and (C10), one may write

$$h(z,t)=q(0)\left(t+\frac{t^2}{2}\right)+h(z(t)-vt,0) \tag{C11}$$

Substituting IC: $h(z,0)=h_i+az$ in Equation (C11)

$$h(z,t)=q(0)\left(t+\frac{t^2}{2}\right)+h_i+a(z(t)-vt) \tag{C12}$$

Putting $a=(h_N-h_i)/\lambda(0)$ (assumed) and $h(z=\lambda(t),t)=h_N$ (h_N is enthalpy at boiling boundary) in Equation (C12), one may obtain

$$\lambda(t)=vt+\frac{h_N-h_i-q(0)\left(t+\frac{t^2}{2}\right)}{h_N-h_i}\lambda(0) \tag{C13}$$

In Equation (C13), v is constant, and h_i and h_N are not time-dependent.

NOMENCLATURE

Symbols

c_p	specific heat (J/kg K)
D	diameter of flow channel, m
E	error, dimensionless
f	degree of closeness of numeral solution to exact solution, dimensionless
h	phase enthalpy, J/kg
k	thermal conductivity, W/m K
N	number of computation cells in single-phase liquid zone, dimensionless
p	pressure, N/m^2
T	temperature, K
Pe	Peclet number, dimensionless
Q	heat transfer rate, W/m^3
q	heat transfer rate, W/kg
r	grid refinement ratio
$q(0)$	heat transfer rate at $t=0$
q''	heat flux, W/m^2
t	time, s
v	phase velocity, m/s

DOI: 10.1002/fld

z	axial length, m
Δz	grid spacing, m

Greek letters

ρ	phase density, kg/m^3
λ	top boundary position of a node from inlet, m
λ	boiling height at $t=0$
$\Delta\lambda_n$	nodal height of nth node $=\lambda_n-\lambda_{n-1}$, m
τ	transportation delay, s
η	order of convergence
ψ	scalar quantity

Subscripts

l	liquid
g	vapor
h	hydraulic
i	inlet
n	node no.
w	wall
sat	saturation
λ, N	boiling boundary

Superscripts

$\prime$	deviation
exact	exact solution

ACKNOWLEDGEMENTS

The authors are highly thankful to M/s Flotherm Consultants (P) Ltd. for giving useful information on the steam generator.

REFERENCES

1. Boure JA, Bergles AE, Tong LS. Review of two-phase flow instability. *Nuclear Engineering and Design* 1973; **25**:165–192.
2. Gonella VDP, Pandey M, Kalra MS. Review of research on flow instabilities in natural circulation boiling systems. *Progress in Nuclear Energy* 2007; **49**:429–451.
3. Paruya S, Dhur GM, Guha C, Saha P. Research on simulation for next millennium. *Proceedings of IIChE Zonal Conference on Status of Chemical Engineering Research in Eastern India*, Kolkata, 24 September 1998.
4. Paruya S, Dhur GM, Guha C, Saha P. *Documentation of Kaiga-1 Real-Time LOCA Simulation Software*, vol. 1. Flotherm Consultants (P) Ltd: Kolkata, India, December 1998.
5. Jensen JM, Tummescheit H. Moving boundary models for dynamic simulations for two-phase flows. *Proceedings of Second International Modelica Conference*, Germany, 18–19 March 2002.
6. Paruya S, Bhattacharya P. Simulation of the effect of boiling boundary on startup performance of a steam generator. *Proceedings of National Seminar on Technology Upgradation in Process Industries*, Haldia Institute of Technology, Haldia, India, 6 August 2004.
7. Paruya S, Bhattacharya P. Numerical simulation of startup performance of a steam–water natural circulation loop. *Proceedings of third BSME–ASME International Conference on Thermal Engineering*, Dhaka, 20–22 December 2006.

DOI: 10.1002/fld

8. van Bragt DDB, De Kruijf WJM, Manera A, van der Hagen THJJ, van Dam H. Analytical modeling of flashing-induced instabilities in a natural circulation cooled boiling water reactor. *Nuclear Engineering and Design* 2002; **215**:87–98.
9. Benedek SD, Drew DA. An analytical study for determining the dynamics of boiling boundary. *International Journal of Heat and Mass Transfer* 1998; **41**:2735–2742.
10. Frepoli C, Mahaffy JH, Hochreiter LE. A moving subgrid model for simulation of reflood heat transfer. *Proceedings of 10th International Conference on Nuclear Engineering*, Arlington, VA, U.S.A., 14–18 April 2002.
11. Garea VB, Drew DA, Lahey Jr RT. A moving-boundary nodal model for the analysis of the stability of boiling channels. *International Journal of Heat and Mass Transfer* 1999; **42**:3575–3584.
12. Zhang W-J, Zhang C-L. A generalized moving-boundary model for transient simulation of dry-expansion evaporators under larger disturbances. *International Journal of Refrigeration* 2006; **29**:1119–1127.
13. Hasan D, Nekhamkin Y, Rosenband V, Elias E, Gany A, Wacholder E. An exact solution for the moving boiling boundary problem. *Nuclear Engineering and Design* 2001; **203**:243–248.
14. Han GY, Secker Jr PA. Mathematical modeling and transient thermal–hydraulic analysis of boiling water reactors. *International Communications in Heat and Mass Transfer* 1999; **26**:899–908.
15. Chang C-J, Lahey Jr RT. Analysis of chaotic instabilities in boiling systems. *Nuclear Engineering and Design* 1997; **167**:307–334.
16. Saha P, Zuber N. Point of net vapor generation and vapor void fraction in subcooled boiling. *Proceedings of the Fifth International Heat Transfer Conference*, Tokyo, Japan, vol. 4, 1974; 175–179.
17. Demirdžić I, Perić M. Space conservation laws in finite volume calculations of fluid. *International Journal for Numerical Methods in Fluids* 1998; **8**:1037–1050.
18. LeVeque RJ. *Numerical Methods for Conservation Laws*. Birkhauser Verlag: Boston, 1992.
19. LeVeque R, Russell RD, Ruuth S. *Final Report-Conference on Computational Techniques for Moving Interfaces*, Banff, AB, Canada, 23–28 August 2003.
20. Patankar SV. *Numerical Heat Transfer and Fluid Flow*. Hemisphere Publishing Corporation: Washington, 1980.
21. Thomas PD, Lombard CK. Geometric conservation law and its application to flow computations on moving grids. *AIAA Journal* 1979; **17**:1030–1037.
22. Zhang H, Reggion M, Trépanier JY, Camarero R. Discrete form of GCL for moving meshes and its applications in CFD schemes. *Computers and Fluids* 1993; **22**:9–23.
23. Zwart PJ. The integrated space–time finite volume method. *Ph.D. Thesis*, University of Waterloo, 1999.
24. Zwart PJ, Raithby GD, Raw MJ. An integrated space–time finite volume method and its application to moving boundary problems. *Journal of Computational Physics* 1999; **154**:497–519.
25. Demirdžić I, Perić M. Finite volume method for prediction of fluid flow in arbitary shaped domains with moving boundaries. *International Journal for Numerical Methods in Fluids* 1990; **10**:771.
26. Kim D, Choi H. A second-order time-accurate finite volume method for unsteady incompressible flow on hybrid unstructured grids. *Journal of Computational Physics* 2000; **162**:411–428.
27. Chen AJ, Kallinderis Y. Adaptive hybrid (prismatic-tetrahedral) grid for incompressible flows. *International Journal for Numerical Methods in Fluids* 1998; **26**:1085.
28. Ham FE, Lien FS, Strong AB. A fully conservative second-order finite difference scheme for incompressible flow on nonuniform grids. *Journal of Computational Physics* 2002; **177**:117–133.
29. Saha P. Thermally induced two-phase flow instabilities, including the effect of thermal non-equilibrium. *Ph.D. Thesis*, Georgia Institute of Technology, Atlanta, 1974.
30. Levy S. Forced convection subcooled boiling—prediction of vapor volumetric. *International Journal of Heat and Mass Transfer* 1967; **10**:951–965.
31. Thomas J. *Numerical Partial Differential Equations*: *Conservation Laws and Elliptic Equations*. Springer: New York, 1999.
32. Roache PJ. *Fundamentals of Computational Fluid Dynamics*. Hermosa Publishers: Albuquerque, NM, 1998.

DOI: 10.1002/fld